Fluorescence emission patterns near glass and metal-coated surfaces investigated with back focal plane imaging

Alexa L. Mattheyses
University of Michigan
Biophysics Research Division
Ann Arbor, Michigan 48109

Daniel Axelrod
University of Michigan
Biophysics Research Division
Ann Arbor, Michigan 48109
and
University of Michigan
Department of Physics
Ann Arbor, Michigan 48109

Abstract. Often fluorophores observed by microscopy are located close to a planar surface as in total internal reflection microscopy or single molecule studies. The optical properties of fluorescence excitation and emission near a planar surface (possibly metal film coated) between two dielectrics are well understood from the viewpoint of classical electromagnetic theory. We present an experimental method whereby the angular dependence of the emission pattern of a fluorophore near a bare surface or a metal film coated surface that supports surface plasmon resonance can be measured with microscope optics. The technique involves an alteration of the microscope optics to directly record (on a digital CCD camera) the intensity pattern at the objective's back focal plane, which directly maps the angular emission pattern of fluorescence. The experimental emission profile on both glass and aluminum-coated surfaces is anisotropic with a peak at either the critical angle or both the critical angle and the surface plasmon angle. The observed profiles agree well with computer calculations and suggest some optical modifications that are potentially useful in cell biophysics.
[DOI: 10.1117/1.2052867]

Keywords: back focal plane; surface plasmon resonance; high-aperture objective; microscopy.

Paper 05010R received Jan. 13, 2005; revised manuscript received Apr. 25, 2005; accepted for publication Apr. 29, 2005; published online Sep. 19, 2005.

1 Introduction

Fluorescence microscopy is used for probing a wide variety of biological and biophysical questions. Frequently these investigations involve fluorophores in close proximity to the coverslip, either because they are immobilized there as in single molecule studies and surface biochemistry studies or because they are located on a biological cell component (e.g., the plasma membrane) near the growth substrate. The emission properties of fluorophores near an interface between two materials of differing dielectric constants (e.g., sample and coverslip) are different from the isotropic emission of fluorophores in free space. It is important to understand how fluorescence emission properties, including angle-dependent intensity, collected power, polarization, and lifetime, are affected by a fluorophore's distance from and orientation with respect to an interface. The changes in these properties are important both for correctly interpreting experimentally collected data and for suggesting novel experimental designs exploiting the deviations from free space conditions. Various aspects of fluorescence emission properties have been investigated for fluorophores near a glass surface, including changes in fluorescence lifetime[1] and total radiated power.[2] Effects on the angular emission pattern have been theoretically investigated by modeling a fluorophore as a fixed amplitude dipole.[3–6] Hellen and Axelrod[7] described a fixed power dipole model and presented theoretical results for observation angle-dependent intensity as a function of the fluorophores orientation and distance from the surface, as well as for total emission power collected through a high-aperture microscope objective.

Coating the surface with metal provides a dramatic way to alter a fluorophore's emission properties. For an excellent and broad review of most aspects of this subject see the series of papers from the Lakowicz group.[8–12] For fluorophores greater than 500 nm from an interface, interference between propagating light and its reflections off the surface dominates.[13,14] If a fluorophore is within 10 nm of a metal-coated dielectric surface, the metal shortens the fluorescence lifetime and quenches fluorescence.[15] Fluorophores between 10 and 500 nm from a metal surface can transfer much of their energy into exciting surface plasmon modes in the metal.[16–20] This coupling produces an observable hollow cone of radiation propagating into the dielectric supporting the metal film, with a specific half-angle determined by the wavelength of the light and the dielectric constants of the metal, the sample, and the supporting dielectric material[21] (usually a glass coverslip). This effect has been theoretically predicted and experimentally demonstrated in a non-microscope configuration by cou-

Address all correspondence to Alexa L. Mattheyses, Biophysics Research Division, University of Michigan, Ann Arbor, MI, 48109, USA. Tel: 734-647-1828; Fax: 734-764-3323; E-mail: amatthey@umich.edu.

1083-3668/2005/10(5)/054007/6/$22.00 © 2005 SPIE

pling the emission into a hemispherical or hemicylindrical prism.[11,17]

This highly efficient coupling has been used to both increase sensitivity by allowing collection of a large fraction of the total emission from a fluorophore and to decrease background signals from fluorophores far from the surface in spectroscopy, a technique called surface plasmon coupled emission (SPCE).[10,11,22] The increase in signal strength from the coupling between the fluorophore and the metal, decrease of background fluorescence from fluorophores in the bulk solution, and ability to spectrally discriminate signals that accompanies SPCE has proven useful in both DNA hybridization assays[23] and immunoassays.[24,25]

The use of a coupling prism for SPCE can be highly efficient and also allows spectral analysis of biochemical samples. But for some applications, particularly in cell biology, it may be desirable to collect the SPCE light in a configuration from which it can be easily re-imaged. As a step toward that goal, this paper demonstrates the existence of the hollow cone of surface plasmon-generated light, and measures its intensity as a function of polar angle, as collected through a commercial microscope with a high-aperture objective. The angular dependence of fluorescence emission from fluorophores near both glass and metal-coated surfaces is nontrivial, and we display the intensities that are collected by a high-aperture microscope optics as a function of polar angle. We compare experimental results with idealized theoretical results obtained from Hellen and Axelrod's model of a fixed power dipole.

The intensity pattern at the back focal plane (BFP) (also known as the "aperture plane") of the microscope can be used as a map of angular emission patterns. The angle at which emission light emerges from the supporting coverslip corresponds directly to its radial position in the back focal plane. Lieb et al.[26] used a similar method of imaging the back focal plane to determine the orientation of single molecules from their anisotropic angular emission profiles. In our system, we image large ensembles of molecules that provide enough photons to permit higher magnification and resolution of the BFP and consequently more precision in identifying features of the emission patterns. This paper does not deal with single molecules nor attempt to discriminate molecule orientation. Instead, we use the BFP image to investigate the angular emission profile of an ensemble of fluorophores near a glass or metal-coated surface.

Direct imaging of the back focal plane of the microscope objective is accomplished by an arrangement that is rapidly interchangeable with standard sample plane imaging. The intensity versus angle relationship of emitted light is recorded digitally at the back focal plane for samples of both fluorophores on bare glass and on aluminum-coated glass. The experimental angular emission patterns agree well semi-qualitatively with computer calculations based on the theoretical expressions provided by Hellen and Axelrod.[7]

2 Materials and Methods

2.1 *Sample Preparation*

The fluorophore emission properties near two different types of surfaces, glass and aluminum-coated glass, were investigated. In both cases, the fluorescent sample was designed to mimic the optical properties (size and refractive index) that are roughly typical of a fluorescent biological cell. The sample consisted of large diameter (d=8.89 μm) silica beads (Bangs Laboratories, Inc., Fishers, IN). (The refractive index is advertised as 1.37; we measured it by scattering minimization in a glycerol/water solution to be 1.42.) The beads were made fluorescent by coating their surface with 3,3′-dioctadecylindocarbocyanine (diI-C_{18}-3, diI, Molecular Probes, Inc., Eugene, OR) simply by immersion in a diI-ethanol solution and then rinsing with water. The beads were suspended in pure water and allowed to settle on the surface. Therefore, the fluorophore distances from the surface ranged from z=0 to z=8.89 μm. The surface was either a plain glass coverslip or a glass coverslip coated in aluminum. Glass coverslips were coated with 13-, 20-, 25-, or 30-nm of aluminum using a vacuum evaporator.

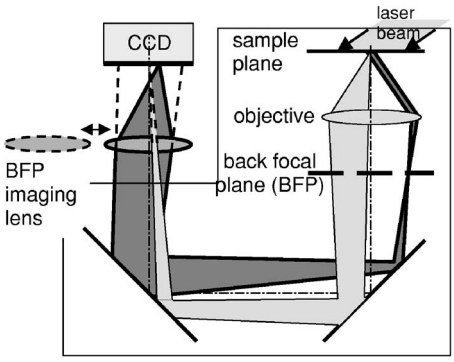

Fig. 1 Optical configuration. The function of a BFP imaging lens, added externally to the optics of an inverted microscope. The path of typical parallel rays emanating from a range of sample points but all at a particular angle is shown with dark gray shading; the path of typical rays with a range of angles but all emanating from a single point of the sample is shown with light gray shading. With the BFP imaging lens in place, the microscope's BFP is imaged at the face of the CCD array. With the BFP imaging lens removed from the path, the microscope's sample plane is focused at the face of the CCD array. Ray paths for the BFP lens inserted are shown as solid; for the lens removed they are shown as dashed. This schematic of an inverted microscope's optical system is highly simplified: none of the fixed intermediate lenses and their consequent intermediate focal planes after the objective are depicted. The placement of these intermediate elements varies with manufacturer, finite versus infinite tube length, and inverted versus upright configuration.

2.2 *Optical Configuration*

An inverted microscope (Leitz Diavert) was modified with the insertion of a converging lens, referred to as the back focal plane (BFP) imaging lens, external to the microscope body but before the CCD camera (see Fig. 1). This lens focuses an image of the BFP (instead of an image of the sample plane) on the CCD chip. The BFP imaging lens' focal length and placement were selected by bringing the phase ring of a phase contrast objective into focus in the CCD camera. Once selected, the BFP imaging lens was placed on a slider so it can be easily inserted and removed from the optical path, allowing straightforward imaging of both the BFP and the sample plane of the same sample. The sample was excited with 488-nm laser light at an angle from above. This non-epi-illumination configuration was chosen both to minimize re-

flected excitation light back into the emission path by the metal-coated coverslips and transmission of excitation light into the emission path by regular coverslips. Fluorescence from the sample was collected by a 1.4 NA 63× objective. This illumination-from-above system did not require a dichroic mirror. However, a long-pass colored glass barrier filter (Corning) blocked scattered 488-nm light while transmitting fluorescence at wavelengths greater than 520 nm. The images were recorded with a Star-1 CCD camera (384×576 pixels, Photometrics, now part of Roper Scientific, Tucson, AZ).

2.3 *Image Acquisition and Analysis*

Images of the back focal plane were recorded with exposure times ranging from 0.2 to 5 sec depending on the illumination intensity and brightness of the sample. Images were acquired with the bottom of the beads at the sample/coverslip interface in focus. All image analysis was done with custom-written programs in Interactive Data Language (IDL, Research Systems, Boulder, CO). The final goal of the image analysis was to obtain the fluorescence intensity as a function angle of emission. To achieve this, first the center of the circularly symmetric back focal plane image was found by manually selecting four points on the perimeter of the circle. Four different circles are defined by these points; their computed center points were averaged to give the center of the back focal plane image. Then, for every pixel within a thin ring at a given distance r from the center, an average intensity was calculated.

2.4 *Theory*

To semi-qualitatively compare experimental results with those predicted by theory [Hellen and Axelrod,[7] Eq. (42)], an IDL program was written to theoretically calculate the collected fluorescence that would be observed at various angles θ (measured from the normal to the surface) from a fixed-power dipole situated near a dielectric boundary. The experimental intensities (as a function of θ) were additionally corrected by a standard energy conservation factor[27,28] $(1/\cos\theta)$ to correct for rays incident upon the objective at an oblique angle, before comparison with the theoretical predictions.

The microscope objective essentially maps angles of ray propagation from an in-focus source into off-axis radial positions at the BFP. A consequence of the general "sine condition" for spherical refracting surfaces[27,28] is that a ray originating from an in-focus source on-axis at the focal plane and propagating at an angle θ with respect to the axis will cross the objective's back focal plane at an off-axis radial distance r given by:

$$r = n_3 f \sin\theta \tag{1}$$

where f is the focal length of the objective and n_3 is the refractive index of the medium in which θ is measured (here, the immersion oil and coverslip at $n_3=1.515$). However, since neither the focal length nor the magnification factor for forming a CCD image of the BFP are well known, Eq. (1) shows only the function dependence of r versus θ but not the scaling. The scaling is set here by noting that both the theory and the experimental results show a strong emission intensity maximum at the "critical angle" θ_c at which a skimming ray in the water environment of the fluorophore (index $n_1=1.33$) refracts into the glass coverslip (index n_3). That angle is

$$\theta_c = \sin^{-1}(n_1/n_3). \tag{2}$$

In the experiments here, $\theta_c=61.39$ deg. The measured r values (in number of pixel widths) was scaled to their equivalent θ values by using Eq. (1) and matching the position of the experimental data's distinct peak to the distinct theoretical peak at $\theta_c=61.39$ deg.

Each theoretical calculation assumes a particular set of fluorophore distances, orientations, and emission wavelength, whereas the experimental sample here consists of a complex mix of distances, orientations, wavelengths, local excitation intensities, and collection efficiencies (since some of the fluorophores reside in out-of-focus planes). In addition, the fluorescent-labeled sphere presents an additional curved interface nearby to the fluorophores that is not included in the theory. The fluorescent sphere sample used here mimics many samples of interest in biochemistry and cell biology, which also present such a mix. For example, some fluorescently labeled membranes can be highly orientationally ordered[29] and flat while others are not ordered at all and irregular in conformation, and the cell's refractive index is heterogeneous and in general higher than the surrounding extracellular buffer. Because of these complexities, of which the relative weightings are not well known, a completely quantitative comparison of the angular dependence of emission intensity between theory and experiment is not possible. However, the overall shapes and relative location of peaks still can be compared between theory and experiment, and confirmation of those features can serve as a guide to experimental design.

3 Results

Fluorescent beads were observed and images of the back focal plane were recorded. Then the angular emission profiles were determined from the BFP as described above. An example of the raw BFP data is shown in Fig. 2(A) for a sample on glass and Fig. 2(B) for a sample on aluminum coated glass. For comparison, only half of the BFP from each is shown (at no loss of information because it is azimuthally uniform). Each distance r from the center corresponds to an emission angle θ, and the brightness at each r corresponds to relatively how much fluorescence was emitted and collected at the corresponding angle θ. As r increases, θ increases. The differences between metal and glass can be seen qualitatively. On glass there is a single bright band that occurs at the critical angle after which the fluorescence intensity drops off very quickly to nearly zero. In contrast, on aluminum there are two bright peaks, one at the critical angle and a second corresponding to the surface plasmon angle.

These results are displayed for a partially quantitative comparison by plotting intensity as a function of distance from center as described in Sec. 2. A plot obtained from a single BFP image on bare glass is shown in Fig. 3. The sharp peak of emission occurs at the radius corresponding to the critical angle after which the fluorescence declines sharply. A similar plot was seen for the BFP of every fluorescent bead analyzed ($n=10$). This corresponds well with the theoretical prediction of the angular emission pattern for a perpendicularly oriented fluorophore 500 nm from the surface and ob-

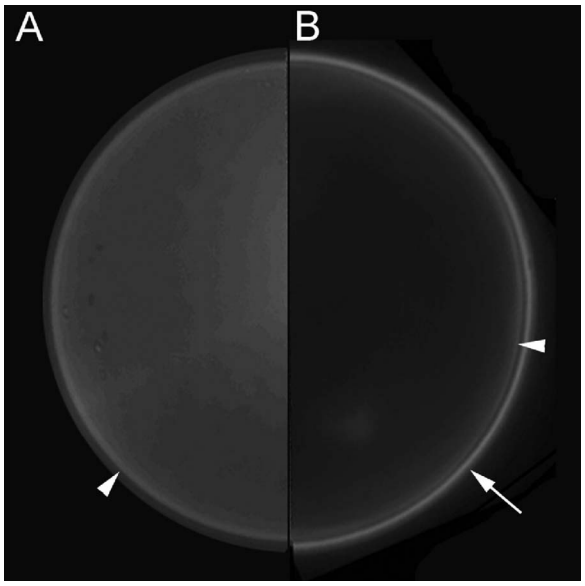

Fig. 2 Experimental images of the back focal plane. (A) Back focal plane of fluorescent sample on bare glass. Arrowhead indicates intensity peak at the critical angle. (B) Back focal plane of fluorescent sample on coverslip coated with 20 nm of aluminum. Arrowhead indicates intensity peak at the critical angle at the same radius as on the bare glass and the full arrow indicates the peak at the surface plasmon angle, at a larger radius and thus larger angle.

served by a 1.4 NA objective (same parameters used for all theoretical calculations) calculated as described in Sec. 2.

Slides were coated with three different thicknesses (t=13, 20, and 30 nm) of aluminum because thickness is one of the parameters that affects surface plasmon coupling. Intensity versus angle plots for the aluminum-coated coverslips are shown in Fig. 4. The experimental data shown in each panel of Fig. 4 derive from a single BFP image, but the features were seen in every image analyzed for the given condition (ranging from n=5 to n=15). Fluorescence from the t =13 nm sample had only one peak of emission, at an angle corresponding to the critical angle [Fig. 4(a)]. This agreed with the theory [Fig. 4(a)]. By t=20 nm, two peaks are visible in both the experimental and theoretical results: the critical angle peak and a surface plasmon peak [Fig. 4(b)]. The surface plasmon peak remains visible at t=30 [Fig. 4(c)], also as predicted by theory.

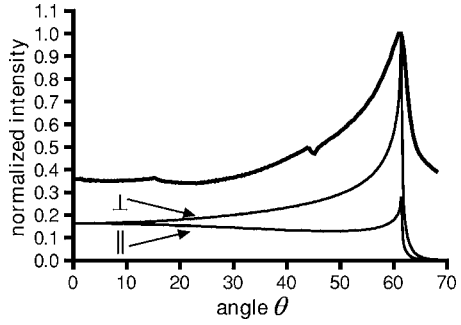

Fig. 3 Normalized emission intensity vs angle for a fluorophore near a glass surface. The experimental data, corrected with the energy conservation factor (1/cos θ), is plotted with the thick line; the theoretical profiles for both perpendicular and parallel oriented dipoles are plotted with thin lines and labeled accordingly.

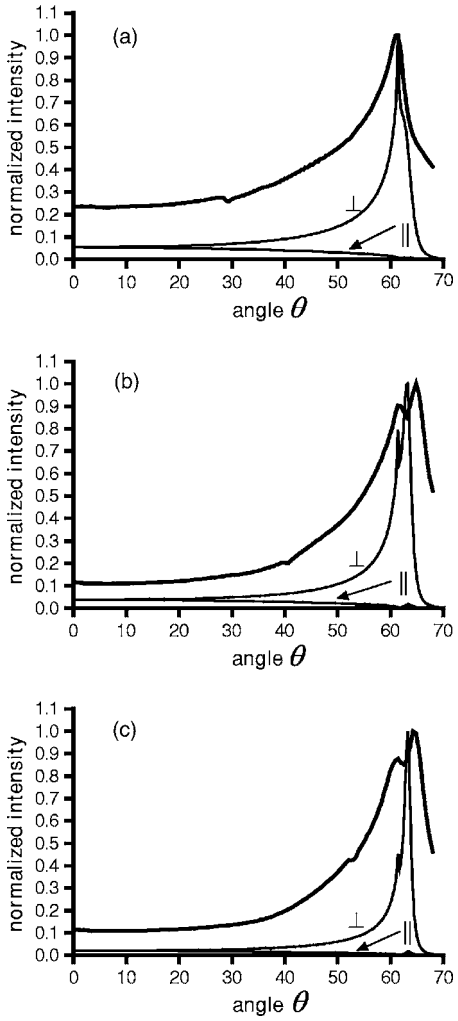

Fig. 4 Normalized emission intensity vs angle for a fluorophore near an aluminum-coated surface. The experimental data, corrected with the energy conservation factor (1/cos θ), is plotted with the thick line; the theoretical profiles for both perpendicular and parallel oriented dipoles are plotted with thin lines and labeled accordingly. (a) 13-nm thick aluminum film; (b) 20-nm thick aluminum film; (c) 30 -nm thick aluminum film.

4 Discussion

We have experimentally investigated angular emission patterns of fluorophores in close proximity to both glass and metal-coated surfaces, by direct digital imaging of the back focal plane of a commercial microscope. The emission patterns are seen to be highly anisotropic, with a disproportionately large fraction of the total fluorescence collected near the critical angle (for bare glass) or near both the critical angle and the surface plasmon angle (for aluminum-coated glass). Clearly, high-aperture objectives (NA$>$1.33) that can capture one or both of these peaks are much better light collectors than even slightly lower aperture objectives that necessarily

miss both of them (NA<1.33). The major features of the results correspond very well with those predicted by theory.

The quantitative differences between the experimental and theoretical results arise in part from several simplifications made in the theoretical work. The theoretical calculations were limited to a particular fluorophore dipole orientation. (Results for orientations both perpendicular and parallel to the surface are shown.) The perpendicular orientation dominates even in a randomly oriented sample because a dipole orientated parallel to the interface has at least 10× less intensity into emission angles close to the critical angle than one oriented perpendicularly. (However, the efficiency of excitation is another matter, depending on the polarization of the excitation.) The theoretical calculation also assumed that the dipoles all reside at a fixed distance from the surface: 500 nm. A distance of about 500 nm theoretically maximizes the coupling into surface plasmon emission, but the experimental sample contains fluorophores at all distances between 0 to almost 9 μm. Thus our experimental results come from an averaging over many fluorophore orientations and positions as opposed to a single one. Also, the theoretical results assume a vacuum emission wavelength 563 nm while the experimental sample produced a band with substantial power between 520 and 600 nm. This experimental wavelength spread would be expected to produce a slight spreading out of the peaks. Another theoretical simplification is the assumption of a single planar interface (bare glass or metal-coated glass) in the vicinity of the fluorophore. In our experiments, and also in typical experiments in cell biology, the fluorophore resides on a curved object of somewhat higher refractive index than the surrounding liquid (although not as high as that of the planar interface).

In all of the images with dual peaks, the separation between the peaks appears somewhat greater than expected from theory. This is probably caused by distortion in the image formed by the BFP imaging lens, a simple lens not corrected for aberrations.

Although the intensity peaks at high angle θ are quite prominent in both theory and experiment, the actual objective does seem relatively more efficient at gathering the lower angle light (even after correction for energy conservation). This partially leads to the seemingly higher relative fluorescence at subcritical angles to the peak at the critical angle for the experimental samples compared to the theory samples. It is possible that an objective loses relatively more high-angle light in surface reflections at its many internal interfaces.

The experimental confirmation of the highly anisotropic emission pattern from a fluorophore into the substrate and its capture by a microscope objective can have several practical consequences for biological microscopy and may guide the development of innovative new microscopy techniques. As mentioned, these results show the utility of using a high-NA objective with bare glass substrates to gather the major peaks of intensity at large angles. This is especially important for experiments where signal/noise needs to be improved. For a typical glass surface, the objective should be chosen so NA $>n_s$ (where n_s is the refractive index of the material in which the fluorophores are imbedded, e.g., the cell cytoplasm or external buffer). This will ensure that the emission peak around the critical angle is collected. Another feature clearly shown in the results is the presence of light propagating at angles larger than θ_c, for both bare and metal-coated glass. This light entirely emanates from fluorophores near the surface, near enough for the dipole "near field" to interact with the bare or metal-coated glass. These surface-proximal molecules can be imaged selectively by blocking all the subcritical angle light emission.[30] The ability to preferentially gather light from surface-proximal molecules has been the motivation for the design of a special paraboloid objective lens.[31]

Interesting possibilities exist for emission-generated surface plasmons at metal-coated coverslips in single-molecule imaging applications, although they have not yet been implemented. Two of the major problems in single molecule detection are low light level and bleaching, and both can be ameliorated simultaneously here. The ability to direct a large portion of emitted light into a hollow cone that can be entirely gathered by a high-aperture objective should greatly improve collection efficiency. In addition, the existence of a surface plasmon generation route will shorten the fluorescence lifetime and thereby render the single molecule fluorophore less bleachable.

When selecting a metal for such a purpose, there are two important considerations. First, the metal should be "good" at supporting surface plasmons that efficiently (i.e., without too much loss into heat) produce a hollow cone of light into the dielectric substrate. Second, the half-angle of the cone of surface plasmon coupled radiation must be small enough to be collected by the microscope objective lens. Whether a particular metal/objective combination will work for a given objective NA can be easily determined by plugging in the dielectric constants of the sample (ε_1) and the metal (ε_2) at the appropriate wavelength into the following inequality:

$$\mathrm{NA} > \mathrm{Re}[\varepsilon_1\varepsilon_2/(\varepsilon_1+\varepsilon_2)]^{1/2}.$$

Silver is one of the most desirable metals from an optical viewpoint, but may not be practical in uncoated form for biological samples because its surface oxidizes very quickly. Gold is the best choice for biological samples, as it is also very good at supporting surface plasmons, and will not suffer ill effects from exposure to samples. Gold, however, requires too large of a half-angle to be collected by our 1.4-NA objective. Higher aperture objectives, such as NA$=1.53$ or greater, are suitable for collecting the surface plasmon resonance created on a gold surface. Therefore aluminum was chosen for this study, because it fulfills both of the criteria. The surface plasmon half-angle for aluminum at $\lambda=563$ occurs at $\theta=63$, which corresponds to a numerical aperture of 1.35. Another benefit of aluminum is that it can be derivatized by organosilanes for many desired chemical functionalities.[32]

Apart from the generation of surface plasmons, metal coatings give rise to a strong fluorescence quenching effect and consequently decreased fluorescence lifetime for fluorophores at small distances (0 to 2 nm). This quenching decreases rapidly in effectiveness at larger distances and is negligible at 10 nm (where surface plasmon generation becomes most effective). This powerful but short-range quenching ability can potentially be used to separately investigate the leaflets of a fluorescently labeled lipid bilayer supported on metal-coated glass. If the bilayer is bleached by a brief flash of illumination with a high-intensity laser, the fluorophores in the distal leaf-

let (d=7 nm) will bleach most rapidly because those in the proximal leaflet (d=2 nm) have a shortened lifetime and will not bleach as efficiently. Under subsequent dimmer illumination conditions, fluorophores within 2 nm of the metal (i.e., the proximal leaflet) will have their fluorescence quenched. The postbleach rate of fluorescence recovery then will report the rate of transmembrane lipid "flip-flop."

The use of metal-enhanced fluorescence in spectroscopy is a field that has had much interest lately, as discussed by Lakowicz et al.[8–12,33] Fluorophores near metal have been observed to have a distance-dependent decrease in fluorescence lifetime as well as an increase in quantum yield, which leads to increased brightness and improved photostability.[33] These increases have been shown in a variety of systems including fluorescently labeled proteins[34] and DNA.[35] A combination of these alterations in radiative decay rate along with surface plasmon peak collection in a microscope could lead to some powerful imaging techniques.

A related theoretical area needs further work: what is the effect of the anisotropic emission intensity pattern on optical resolution? The familiar Raleigh condition relating minimum resolvable distance to numerical aperture is derived under the assumption that the intensity reaching the objective is uniform across its face. As shown experimentally here, this assumption is manifestly untrue, so the theoretically expected resolution should differ from the predictions of the standard Raleigh expression.

Acknowledgments

This work was supported by National Institutes of Health (NIH) grant no. R01-NS38129 to D.A. and a NIH Molecular Biophysics Training Grant Fellowship and a Guidant Award Fellowship to A.L.M.

References

1. W. Lukosz and R. E. Kunz, "Fluorescence lifetime of magnetic and electric dipoles near a dielectric interface," *Opt. Commun.* **20**(2), 195–199 (1977).
2. W. Lukosz and R. E. Kunz, "Light emission by magnetic and electric dipoles close to a plane interface. I. Total radiated power," *J. Opt. Soc. Am.* **67**(12), 1607–1614 (1977).
3. W. Lukosz and R. E. Kunz, "Light emission by magnetic and electric dipoles close to a plane dielectric interface. II. Radiation patterns of perpendicular orientated dipoles," *J. Opt. Soc. Am.* **67**(12), 1615–1619 (1977).
4. C. K. Carniglia, L. Mandel, and K. H. Drexhage, "Absorption and emission of evanescent photons," *J. Opt. Soc. Am.* **62**(4), 479–486 (1972).
5. T. P. Burghardt and N. L. Thompson, "Effect of planar dielectric interfaces on fluorescence emission and detection," *Biophys. J.* **46**, 729–737 (1984).
6. E.-H. Lee, R. E. Benner, J. B. Fen, and R. K. Chang, "Angular distribution of fluorescence from liquids and monodispersed spheres by evanescent wave excitation," *Appl. Opt.* **18**, 862–868 (1979).
7. E. H. Hellen and D. Axelrod, "Fluorescence emission at dielectric and metal-film interfaces," *J. Opt. Soc. Am. B* **4**(3), 337–350 (1987).
8. J. R. Lakowicz, "Radiative decay engineering: Biophysical and biomedical applications," *Anal. Biochem.* **298**, 1–24 (2001).
9. J. R. Lakowicz, Y. Shen, S. D'Auria, J. Malicka, J. Fang, Z. Gryczynski, and I. Gryczynski, "Radiative decay engineering 2. Effects of silver island films on fluorescence intensity, lifetimes, and resonance energy transfer," *Anal. Biochem.* **301**, 261–277 (2002).
10. J. R. Lakowicz, "Radiative decay engineering 3. Surface plasmon-coupled directional emission," *Anal. Biochem.* **324**(2), 153–169 (2004).
11. I. Gryczynski, J. Malicka, Z. Gryczynski, and J. R. Lakowicz, "Radiative decay engineering 4. Experimental studies of surface plasmon-coupled directional emission," *Anal. Biochem.* **324**(2), 170–182 (2004).
12. J. R. Lakowicz, "Radiative decay engineering 5: Metal-enhanced fluorescence and plasmon emission," *Anal. Biochem.* **337**, 171–194 (2005).
13. K. H. Drexhage, "Interaction of light with monomolecular dye layers," *Prog. Opt.* **12**, 163–232 (1974).
14. K. H. Drexhage, "Influence of a dielectric interface on fluorescence decay time," *J. Lumin.* **12**, 693–701 (1970).
15. A. Camplon, A. R. Gallo, C. B. Harris, H. J. Robota, and P. M. Whitmore, "Electronic energy transfer to metal surfaces: A test of classical image dipole theory at short distances," *Chem. Phys. Lett.* **73**(3), 447–450 (1980).
16. G. W. Ford and W. H. Weber, "Electromagnetic interactions of molecules with metal surfaces," *Phys. Rep.* **113**, 195–287 (1984).
17. W. H. Weber and C. F. Eagen, "Energy transfer from an excited dye molecule to the surface plasmons of an adjacent metal," *Opt. Lett.* **4**(8), 236–238 (1979).
18. H. Kuhn, "Classical aspects of energy transfer in molecular systems," *J. Chem. Phys.* **53**, 101–108 (1970).
19. M. R. Philpott, "Effect of surface plasmons on transitions in molecule," *J. Chem. Phys.* **62**, 1812–1817 (1975).
20. T. Tamir, J. J. Burke, and G. I. Stegeman, "Surface-polarization-like waves guided by thin lossy metal films," *Phys. Rev. B* **33**, 5186–5201 (1986).
21. H. Raether, *Surface Plasmons on Smooth and Rough Surfaces and on Gratings*, Springer-Verlag, New York (1988).
22. J. R. Lakowicz, J. Malicka, I. Gryczynski, and Z. Gryczynski, "Directional surface plasmon-coupled emission: A new method for high sensitivity detection," *Biochem. Biophys. Res. Commun.* **307**(3), 435–439 (2003).
23. J. Malicka, I. Gryczynski, Z. Gryczynski, and J. R. Lakowicz, "DNA hybridization using surface plasmon-coupled emission," *Anal. Chem.* **75**(23), 6629–6633 (2003).
24. E. Matveeva, J. Malicka, I. Gryczynski, Z. Gryczynski, and J. R. Lakowicz, "Multi-wavelength immunoassays using surface plasmon-coupled emission," *Biochem. Biophys. Res. Commun.* **313**(3), 721–726 (2004).
25. E. Matveeva, Z. Gryczynski, I. Gryczynski, and J. R. Lakowicz, "Immunoassays based on directional surface plasmon-coupled emission," *J. Immunol. Methods* **286**(1–2), 133–140 (2004).
26. M. A. Lieb, J. M. Zavizlan, and L. Novotny, "Single-molecule orientations determined by direct emission pattern imaging," *J. Opt. Soc. Am. B* **21**(6), 1210–1215 (2004).
27. R. Oron, J. L. Guedalia, N. Davidson, A. A. Friesmen, and E. Hasman, "Anomaly in a high-numerical aperture diffractive focusing lens," *Opt. Lett.* **25**(7), 439–441 (2000).
28. B. Richards and E. Wolf, "Electromagnetic diffraction in optical systems. II. Structure of the image field in an aplanatic system," *Proc. R. Soc. London, Ser. A* **253**(1274), 358–379 (1959).
29. S. E. Sund, J. A. Swanson, and D. Axelrod, "Cell membrane orientation visualized by polarized total internal reflection fluorescence," *Biophys. J.* **77**(4), 2266–2283 (1999).
30. D. Axelrod, "Selective imaging of surface fluorescence with very high aperture microscope objectives," *J. Biomed. Opt.* **6**(1), 6–13 (2001).
31. J. Enderlein, T. Ruckstuhl, and S. Seeger, "Highly efficient optical detection of surface-generated fluorescence," *Appl. Opt.* **38**(4), 724–732 (1999).
32. R. M. Fulbright and D. Axelrod, "Dynamics of nonspecific adsorption of insulin to erythrocyte membrane," *J. Fluoresc.* **3**, 1–16 (1993).
33. J. R. Lakowicz, C. D. Geddes, I. Gryczynski, J. Malicka, Z. Gryczynski, K. Aslan, J. Lukomska, E. Matveeva, J. Zhang, R. Badugu, and J. Huang, "Advances in surface-enhanced fluorescence," *J. Fluoresc.* **14**(4), 425–442 (2004).
34. B. P. Maliwal, J. Malicka, I. Gryczynski, Z. Gryczynski, and J. R. Lakowicz, "Fluorescence properties of labeled proteins near silver colloid surfaces," *Biopolymers* **70**, 585–594 (2003).
35. J. R. Lakowicz, J. Malicka, and I. Gryczynski, "Fluorescence spectral properties of cyanine dye-labeled DNA oligomers on surfaces coated with silver particles," *Anal. Biochem.* **317**, 136–146 (2003).